Journal of Materials Chemistry A

PAPER

View Article Online
View Journal | View Issue



Cite this: J. Mater. Chem. A, 2014, 2, 18823

# Synthesis and hydrogen adsorption properties of internally polarized 2,6-azulenedicarboxylate based metal–organic frameworks†

Samir Barman,[a] Anupam Khutia,[b] Ralph Koitz,[a] Olivier Blacque,[a] Hiroyasu Furukawa,*[c] Marcella Iannuzzi,[a] Omar M. Yaghi,[cd] Christoph Janiak,[b] Jürg Hutter*[a] and Heinz Berke*[a]

Received 25th August 2014
Accepted 12th September 2014

DOI: 10.1039/c4ta04393f

www.rsc.org/MaterialsA

To improve the binding energy of hydrogen, incorporation of internally polarized organic units into metal–organic frameworks (MOFs) should be a promising strategy. In this study, two novel MOFs composed of internally polarized 2,6-azulenedicarboxylate (2,6-azd), termed MOF-649 [$Zn_2$(2,6-azd)$_2$(dabco), where dabco = 1,4-diazabicyclo[2.2.2]octane] and MOF-650 [$Zn_4O$(2,6-azd)$_3$], have been synthesized, and their crystal structures were determined by single-crystal X-ray diffraction analyses. Both materials displayed permanent microporosity, and the Brunauer–Emmett–Teller (BET) surface areas of MOF-649 and MOF-650 are estimated to be 910 and 2630 $m^2\ g^{-1}$, respectively. The $H_2$ adsorption measurements showed that MOF-650 adsorbs 14.8 mg $g^{-1}$ of hydrogen at 77 K and 1 bar. The polarization effect of the azulene unit in the framework is supported by high initial isosteric heat of adsorption of 6.8 kJ $mol^{-1}$ for MOF-650. A detailed computational analysis using density functional theory was carried out in order to investigate the structure and electronic properties of MOF-650 and subsequently to understand its site-specific interactions with hydrogen.

## 1. Introduction

Metal–organic frameworks (MOFs) are receiving immense attention owing to their unique structural features, the relative ease with which their functionalities may be modified, and their potential applications in gas storage, separation and catalysis.[1] In particular, the discovery of extraordinarily high cryogenic (77 K) total $H_2$ uptake (>10 wt%) by MOFs highlights their potential as ideal storage media for clean energy.[2] However, due to their insufficient interactions with $H_2$, the storage capacity at room temperature is low, which hinders realization of practical usage.[3] To improve MOF interaction energies with $H_2$, utilization of open metal sites and impregnation with alkali metals were proposed.[3–5] Furthermore, it is believed that MOFs with high local charge densities would be accompanied by improved hydrogen adsorption enthalpy.[6] In this context we anticipated that incorporation of internally polarized units into the MOF backbone would lead to enhancement of the polarization potential *via* the Coulombic field of such functionalities, which is expected to improve the binding of $H_2$ locally and/or globally.[7,8]

We envisage that the incorporation of azulene units, as linkers in MOFs, will lead to a strongly polarizing environment as a direct result of azulene's polar character (contrary to isomeric naphthalene units). To this end, we first prepared the organic linker, 2,6-azulenedicarboxylic acid (2,6-$H_2$azd) (Fig. 1a and Scheme S1, ESI†), and subsequently sought to synthesize MOFs possessing secondary building units (SBUs) based on either $Zn_2(CO_2)_4$ paddle-wheels or $Zn_4O(CO_2)_6$ octahedra. This is primarily based on the expectation that the resulting reticulated frameworks will be accompanied by uniformly polarized pore walls, potentially high porosities, and high apparent internal surface areas.[9,10] Here, by applying this strategy, we synthesized two novel frameworks having polarized 2,6-azd units [termed MOF-649: $Zn_2$(2,6-azd)$_2$(dabco) and MOF-650: $Zn_4O$(2,6-azd)$_3$, dabco = 1,4-diazabicyclo[2.2.2]octane]. More specifically, we report the details of the synthetic procedure and structural characterization for MOF-649 and MOF-650

[a]Chemisches Institut, Universitat Zurich, Winterthurerstrasse 190, CH-8057, Zurich, Switzerland. E-mail: hberke@chem.uzh.ch; hutter@chem.uzh.ch; Fax: +41-44-635-6802

[b]Institut für Anorganische Chemie und Strukturchemie, Universität Düsseldorf, 40204 Düsseldorf, Germany

[c]Department of Chemistry, University of California-Berkeley, Materials Sciences Division, Lawrence Berkeley National Laboratory, Kavli Energy NanoSciences Institute at Berkeley, Berkeley, California 94720, USA. E-mail: furukawa@berkeley.edu

[d]King Fahd University of Petroleum and Minerals, Dhahran 34464, Saudi Arabia

† Electronic supplementary information (ESI) available: Scheme S1 (scheme for synthesis of 2,6-$H_2$azd), Fig. S1–S3 (modelled structures of MOF-650 which incorporated different primary $H_2$ binding sites), and Fig. S4 and S5 ($N_2$ isotherm and TGA spectra). CCDC 922543 and 922544. For ESI and crystallographic data in CIF or other electronic format see DOI: 10.1039/c4ta04393f

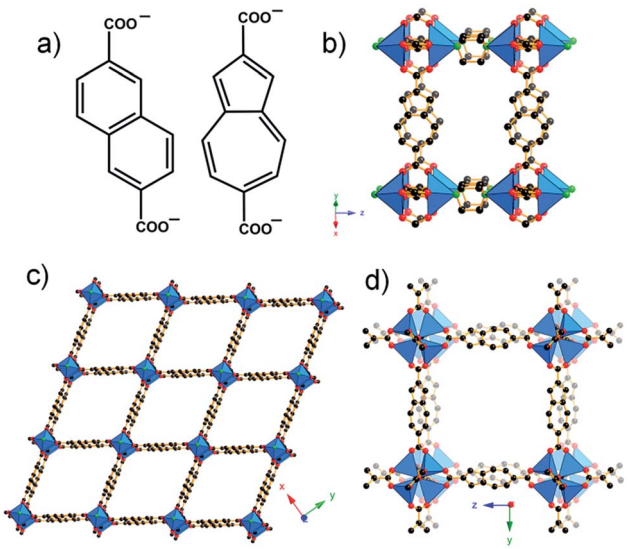


Fig. 1 A view of the linker 2,6-naphthalenedicarboxylate (a, left) and its isomeric unit 2,6-azulenedicarboxylate (a, right). Partial view of the single crystal X-ray structure of MOF-649 exhibiting its 3D framework constructed *via* pillaring the 2D rhombic grids through dabco (b); the primitive cubic net (pcu) in MOF-649 showing its wide open channels of approximately 15.7 × 9.0 Å running along the crystallographic *c* axis (c); and the partial view of the single crystal X-ray structure of MOF-650 exhibiting its pcu topology constructed *via* connection through octahedral shaped $Zn_4O(CO_2)_6$ secondary building units (SBUs) (d). In the case of b, c and d, the orientational disorder of the azulene units was omitted for clarity. Atom colors: Zn, blue polyhedra; O, red; C, black and N, green (for b and c). All hydrogen atoms are omitted for clarity.

accompanied by a discussion on both the porosity and $H_2$ adsorption properties of these MOFs.

Furthermore, we conduct a computational investigation using density functional theory (DFT) to clarify whether the polarization potential of 2,6-azd or the linker-generated hydrogen binding pockets is a greater factor in the adsorption of $H_2$. In particular, we create models for MOF-650 that incorporate several possible primary hydrogen binding sites resulting from the most random arrangements of the asymmetrical 2,6-azd linker around the SBUs. We calculate the corresponding $H_2$ binding energies for MOF-650 and compare them with those for the isostructural IRMOF-8 [$Zn_4O$(2,6-napthalenedicarboxylate)$_3$] containing nonpolar naphthalene linkers.[9,11,12]

# 2. Experimental section

## 2.1 Materials

All commercially available reagents and solvents, such as *N*,*N*-dimethylformamide (DMF), 1-methyl-2-pyrrolidone (NMP), $Zn(NO_3)_2\cdot 6H_2O$, anhydrous acetone, and amylene-stabilized chloroform ($CHCl_3$), were purchased from Aldrich and were used without further purification. Prior to use, diethyl ether ($Et_2O$) and tetrahydrofuran (THF) were dried *via* distillation under a $N_2$ atmosphere using the sodium benzophenone ketyl radical. 2,6-$H_2$azd was prepared according to a published procedure (see Scheme S1, ESI†).[13,14]

## 2.2 Analytical techniques

Single-crystal X-ray diffraction (SXRD) data for MOF-649 and MOF-650 were collected on an Xcalibur diffractometer (Agilent Technologies, Ruby CCD detector) using a single wavelength Enhance X-ray source with Mo-K$\alpha$ radiation, $\lambda = 0.71073$ Å.[15] The powder X-ray diffraction (PXRD) patterns were obtained with a Bruker D8 Advance system equipped with a Cu sealed tube ($\lambda = 1.5406$ Å). The following conditions were applied: 40 kV, 40 mA, increment = 0.007°, and scan speed = 1.5 s per step. Thermogravimetric analysis (TGA) data were obtained on a NETZSCH STA 449C instrument at a heating rate of 1 °C $min^{-1}$ under a $N_2$ atmosphere. Infrared (IR) spectra were recorded on a Perkin-Elmer 1600 Fourier transform spectrometer using KBr pellets with frequencies ($\nu_{max}$) quoted in wavenumbers ($cm^{-1}$). Elemental microanalyses were carried out with a LECO CHNS-932 analyser. $^1$H and $^{13}$C NMR spectra were recorded on a Varian Mercury (200 MHz) spectrometer. The guest free sample of MOF-649 was obtained on a Tousimis Samdri PVT-3D critical point dryer.

## 2.3 Synthesis of $[Zn_2(2,6\text{-azd})_2(dabco)](DMF)_5(H_2O)_2$ (MOF-649)

2,6-$H_2$azd (0.027 g, $1.3 \times 10^{-4}$ mol) and $Zn(NO_3)_2\cdot 6H_2O$ (0.075 g, $2.5 \times 10^{-4}$ mol) were dissolved in 1.8 mL of DMF. Dabco (0.014 g, $1.3 \times 10^{-4}$ mol) was then added to the solution, which immediately produced a large amount of dark blue precipitate. The mixture was filtered using a 60 mL PYREX glass funnel with fine porosity. The filtrate was collected, and the solution was sealed in a 20 mL glass vial. The vial was heated to 85 °C (1 °C $min^{-1}$) for 60 h in a programmable oven and then cooled down to room temperature. The resulting dark blue-green needle-shaped crystals were collected by filtration and washed with DMF (3 × 2 mL). Elemental microanalysis for MOF-649, $[Zn_2(2,6\text{-azd})_2(dabco)](DMF)_5(H_2O)_2 \equiv C_{45}H_{63}O_{15}N_7Zn_2$, calculated (%): C 50.38, H 5.92, N 9.14; found C 50.19, H 6.12, N 8.99. FT-IR (KBr, 4000–400 $cm^{-1}$): 3468 (m, br), 2930 (m, br), 1658 (vs), 1590 (m), 1501 (w), 1350 (vs), 1297 (w), 1251 (w), 1205 (m), 1087 (s), 1048 (m), 1015 (w), 923 (w), 877 (w), 811 (m), 786 (s), 654 (m), 609 (w), 576 (m). To obtain guest free materials, the DMF washed crystals were further washed with $CHCl_3$ (3 × 2 mL) and were subsequently soaked in 10 mL of $CHCl_3$ for 3 days with fresh $CHCl_3$ being added every 24 h. The final $CHCl_3$ exchanged material was then thoroughly washed with anhydrous acetone prior to the activation on a supercritical $CO_2$ drier.[2c]

## 2.4 Synthesis of $[Zn_4O(2,6\text{-azd})_3](DMF)_4(NMP)_4(H_2O)_{13}$ (MOF-650)

2,6-$H_2$azd (0.068 g, $3.1 \times 10^{-4}$ mol) and $Zn(NO_3)_2\cdot 6H_2O$ (0.139 g, $4.67 \times 10^{-4}$ mol) were dissolved in a 8.5 mL mixture of DMF–NMP (1.5 : 1, v/v). The clear dark blue solution was transferred into a 20 mL glass vial and 0.57 mL of EtOH was added. After the vial was tightly capped, it was heated to 90 °C

 

at a rate of 1.5 °C $min^{-1}$ for 60 h in a programmable oven. Cubic-shaped dark blue crystals were separated from the mother liquor contained in the vial and washed with DMF–NMP (1 : 1, v/v) (3 × 5 mL). Elemental microanalysis for the air dried MOF-650, $[Zn_4O(2,6\text{-azd})_3]_8(\text{-DMF})_4(NMP)_4(H_2O)_{13} \equiv C_{320}H_{234}O_{125}N_8Zn_{32}$, calculated (%): C 46.40, H 2.85, N 1.35; found C 45.57, H 3.82, N 2.53. FT-IR (KBr, 4000–400 $cm^{-1}$): 3420 (s, br), 2929 (m, br), 1660 (vs), 1612 (s), 1575 (w), 1489 (w), 1410 (vs), 1360 (w), 1256 (w), 1199 (w), 1100 (w), 925 (w), 790 (s), 660 (w), 584 (w).

To obtain guest-free materials, the DMF–NMP washed crystals were soaked in 10 mL of $CHCl_3$ for 3 days with fresh $CHCl_3$ added every 24 h. The $CHCl_3$ exchanged material was activated at 50 °C for 12 h under dynamic vacuum.

### 2.5 Gas sorption measurements

Low-pressure $N_2$ and $H_2$ adsorption measurements were performed on an Autosorb-1 (Quantachrome)[16] and a Micromeritics ASAP 2020 volumetric gas adsorption analyser, respectively. The samples were outgassed to $10^{-6}$ Torr. Helium was used for the estimation of the dead volume, assuming that it was not adsorbed at any of the studied temperatures. Liquid $N_2$ and liquid Ar baths were used for adsorption measurements at 77 and 87 K, respectively. Ultra-high-purity grade $N_2$, $H_2$, and He (99.999% purity) were used throughout the adsorption experiments.

## 3. Computational details

All DFT calculations were performed with the Quickstep module[18] of the CP2K program package.[19] The exchange–correlation energy was treated with the revised PBE functional[20] and van der Waals contributions were accounted for using the Grimme D3 formalism.[21] Double-zeta valence polarized basis sets of the MOLOPT type[22] and Goedecker–Teter–Hutter pseudopotentials[23] were used for all elements. The electronic density was expanded in plane waves up to a cut-off energy of 500 Ry.

MOFs were modelled as infinite cubic crystals based on a supercell containing eight $Zn_4O(CO_2)_6$ clusters. The cell size of MOF-650 was fixed at the minimum-energy value of $a_0 = 31.0$ Å (1.45% larger than the experimental structure) and that of IRMOF-8 at $a_0 = 30.5$ Å. Hydrogen molecules were adsorbed at the various binding sites and the structure was fully relaxed in order to calculate the adsorption energies.

It is to be noted that van der Waals interactions contribute significantly to the adsorption energies and they are treated in an approximate way with the DFT-D3 approach by Grimme *et al.*[21] This substantially improves adsorption energies compared to a DFT-only treatment.[24] The calculations are carried out at zero Kelvin and for a single adsorbed $H_2$ molecule at a specific site, which neglects any finite-temperature effects and effects of adsorption at multiple or varying sites.

Table 1 Crystallographic data and structural refinement summary for MOF-649 and MOF-650[a]

| | MOF-649 | MOF-650 |
|---|---|---|
| CCDC | 922544 | 922543 |
| Empirical formula | $C_{15}H_{12}NO_4Zn$, $2(C_3H_7NO)$, $H_2O$ | $8(C_{36}H_{18}O_{13}Zn_4)$, $4(C_3H_7NO)$, $4(C_5H_9NO)$, $13(H_2O)$ |
| Formula weight (g $mol^{-1}$) | 499.83 | 8282.98 |
| Wavelength (Å) | 0.71073 | 0.71073 |
| Temperature (K) | 153(2) | 183(2) |
| Crystal system | Orthorhombic | Cubic |
| Space group | *Cmmm* | $Fm\bar{3}m$ |
| $a$ (Å) | 16.052(5) | 30.5557(17) |
| $b$ (Å) | 21.172(5) | 30.5557(17) |
| $c$ (Å) | 9.625(5) | 30.5557(17) |
| $\alpha = \beta = \gamma$ (°) | 90 | 90 |
| Volume ($Å^3$) | 3271(2) | 28 528(3) |
| $Z$ | 4 | 1 |
| Density (calcd) (mg $m^{-3}$) | 1.015 | 0.482 |
| Abs. coefficient ($mm^{-1}$) | 0.783 | 0.686 |
| $F$(000) | 1044 | 4170 |
| Crystal size ($mm^3$) | 0.33 × 0.11 × 0.04 | 0.18 × 0.17 × 0.10 |
| $\theta$ range (°) | 2.5 to 25 | 2.9 to 25.3 |
| Reflections collected | 12 129 | 13 859 |
| Reflections unique | 1650 [$R_{int} = 00.058$] | 1353 [$R_{int} = 0.1979$] |
| Completeness to $\theta$ (%) | 99.8 | 99.9 |
| Absorption correction | Analytical | Analytical |
| Max/min transmission | 0.944/0.701 | 0.481/0.326 |
| Data/restraints/parameters | 1345/21/73 | 744/39/37 |
| Goodness-of-fit on $F^2$ | 1.096 | 1.123 |
| Final $R_1$ and w$R_2$ indices [$I > 2\sigma(I)$] | 0.0719, 0.2138 | 0.1443, 0.3390 |
| $R_1$ and w$R_2$ indices (all data) | 0.0823, 0.2173 | 0.2244, 0.3752 |

[a] Data based on the PLATON/SQUEEZE[17] model.

# 4. Results and discussion

## 4.1 Structural analysis of MOF-649 and MOF-650

**[$Zn_2$(2,6-azd)$_2$(dabco)] (MOF-649).** SXRD analysis reveals that MOF-649 crystallizes in the *Cmmm* space group with $a = 16.052$ Å, $b = 21.172$ Å and $c = 9.625$ Å (Table 1). The framework of MOF-649 is composed of paddle-wheel dinuclear $Zn_2$ units (Fig. 1b), which are bridged by the 2,6-azd dianion to form a 2D rhombic layer structure and further pillared by dabco to lead to an overall 3D structure with primitive cubic (pcu) topology. The carbon atoms of both dabco and the azulene linker of MOF-649 are disordered. MOF-649 possesses channels whose diameter is approximately 15.7 × 9.0 Å along the crystallographic *c* axis (Fig. 1c). If the occluded solvents are removed, a large total solvent accessible void of 68% is estimated.

**[$Zn_4O$(2,6-azd)$_3$] (MOF-650).** MOF-650 crystallizes in a cubic space group with the cell parameter $a = 30.5557$ (Table 1). SXRD analysis reveals that MOF-650 has a 3D framework constructed from the linkage of $Zn_4O(CO_2)_6$ SBUs and the linear ditopic 2,6-azd linker (Fig. 1d). The carbon atoms of the azulene linker of MOF-650 are disordered. The overall connectivity of the framework is similar to the MOF-5 cubic structure.[25] MOF-650 has two types of cavities having approximate diameters of 15 and 18.0 Å and has a large calculated void volume of 86%.

## 4.2 Structural features of MOF-650 from simulations

Due to the asymmetrical structural feature (Fig. 1a, right) it is expected that the 2,6-azd linker may connect around the SBUs of MOF-650 either *via* the carboxylate units of the 5- or the 7-membered ring (Fig. 2 and S1–S3, ESI†). This generates a maximum of four different types of α or β sites in the

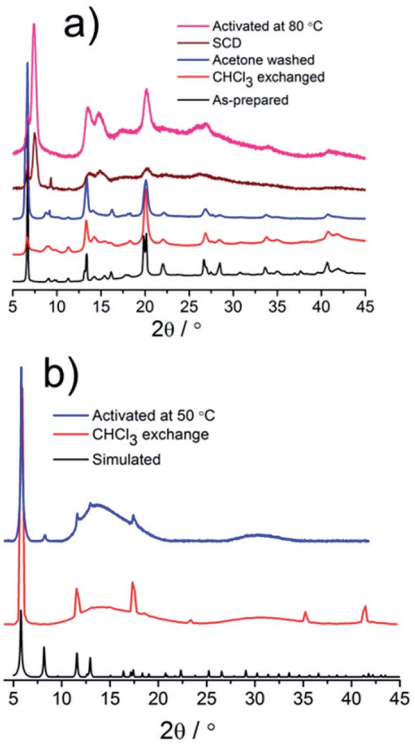


Fig. 3 (a) PXRD patterns of MOF-649: as-prepared (black), $CHCl_3$ exchanged (red), $CHCl_3$ exchanged material washed with anhydrous acetone for 2 h (blue), the material prepared after SCD following acetone exchange for 2 h (wine), the material prepared after degassing the SCD material at 80 °C for 3 h (pink). (b) PXRD patterns of MOF-650: as-prepared (black), after $CHCl_3$ exchange (red) and the activated material obtained after degassing the $CHCl_3$ exchanged material at 50 °C for 12 h.

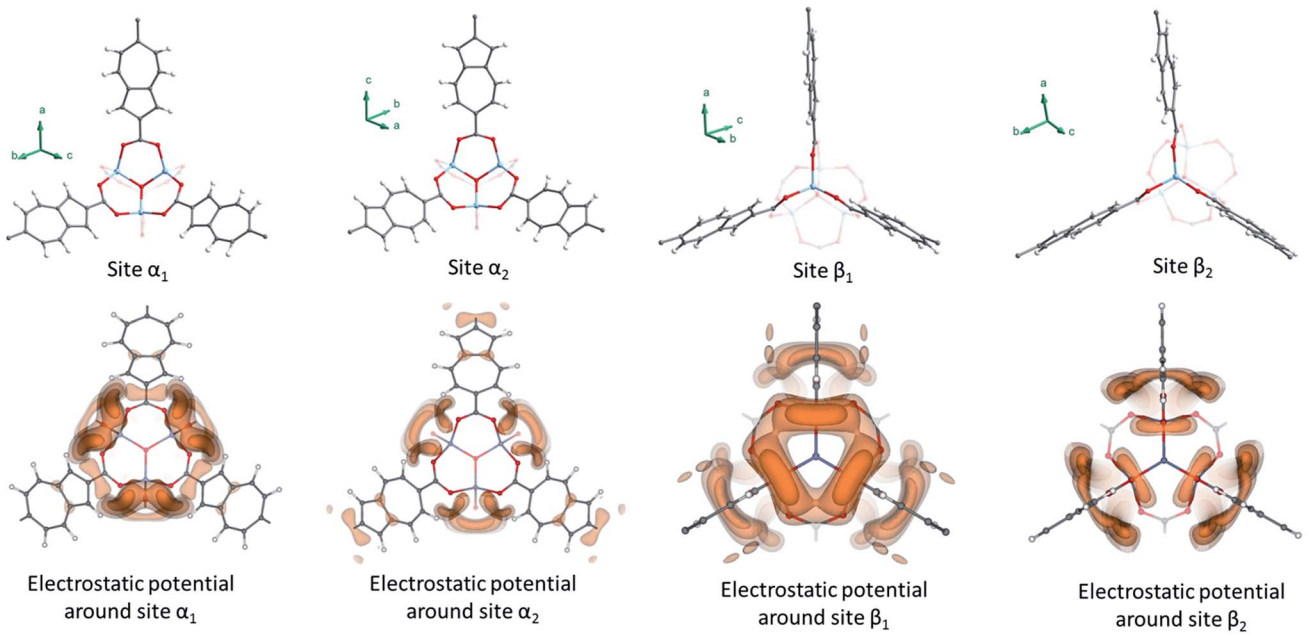


Fig. 2 Partial view of the modeled structure in $Pa\bar{3}$ which incorporates sites $\alpha_1$, $\alpha_2$, $\beta_1$ and $\beta_2$ depending on the number of carboxylate units of 5- or 7-membered ring sides of azulene linkers connected to their edges and their corresponding calculated electrostatic potential (bottom). Atom colors: Zn, blue; O, red; C, black and H, light grey.

 

framework.[11] In the two extreme cases, the α/β sites are coordinated by the carboxylate units of either three 5-membered (which we defined as $\alpha_1/\beta_1$) or three 7-membered ($\alpha_2/\beta_2$) ring sides of the azulene linkers. The remaining two sites arise if the edges of the α/β sites are occupied by two 5-membered and one 7-membered (defined as $\alpha_3/\beta_3$) ring ends of azulene or *vice versa* ($\alpha_4/\beta_4$). To incorporate these sites (Fig. 2 and S1–S3, ESI†) into the MOF-650 framework, we generated two modelled structures in $Pa\bar{3}$ [containing $\alpha_1/\beta_2$, $\alpha_4/\beta_3$ (Fig. S1, top, ESI†) and $\alpha_2/\beta_1$, $\alpha_3/\beta_4$ (Fig. S1, down, ESI†) sites, respectively] and one in $F\bar{4}3m$ [containing both $\alpha_1/\beta_1$ and $\alpha_2/\beta_2$ sites (Fig. S2, ESI†)]. The latter considers an antiparallel arrangement of the linkers with respect to the opposite edge of the square faces of both the cavities. The electrostatic potential around $\alpha_1$, $\alpha_2$, $\beta_1$, and $\beta_2$ and $\alpha_3$, $\alpha_4$, $\beta_3$, and $\beta_4$ sites is depicted in Fig. 2 and S3 (ESI†), respectively. Note the different shape of the potential isosurface depending on the proximity of a 5-membered or 7-membered ring end of the linker.

### 4.3 Permanent porosity of MOF-649 and MOF-650

The $N_2$ isotherm of the activated MOF-649 obtained, after degassing the $CHCl_3$ exchanged sample at room temperature, did not show any significant uptake (Fig. S4, ESI†).[10g] Therefore, efforts were made to activate MOF-649 *via* supercritical $CO_2$ drying (SCD) followed by evacuation at 80 °C.[26] The profile of the $N_2$ isotherm for the activated MOF-649 can be classified as a typical Type I isotherm (Fig. 4a), leading to the presence of permanent microporosity. The Langmuir/BET surface areas and the pore volume of MOF-649 were estimated to be 990/910 $m^2\ g^{-1}$ and 0.35 $cm^3\ g^{-1}$, respectively. These values are larger than those reported for the isostructural framework of DUT-8(Zn).[10g] However, the accessible surface area was still found to lie far below when compared with other pillared MOF analogs.[10d,e,g] In order to find the reasons why the lowered $N_2$ uptake capacity was observed, the PXRD pattern of MOF-649 after SCD was recorded. As demonstrated in Fig. 3a, in conjunction to the peak broadening the new and relatively low intensity peak at $2\theta = 7.3°$, which appears following SCD activation, becomes more intense upon heating at 80 °C, whereas simultaneously the intensity of the peak around $2\theta = 6.7°$ (for (110) reflection) decreases. This implies that the removal of guest molecules causes some structural changes or formation of new phases as shown in an isostructural framework material of DUT-8(Zn).[10g]

The as-prepared MOF-650 was washed with DMF and chloroform, and then occluded solvent molecules were removed under reduced pressure at 50 °C. The peak position of the PXRD pattern of activated MOF-650 was nearly identical to the simulated one (Fig. 3b), which is indicative of the successful activation of the material. To prove the presence of permanent porosity, the $N_2$ sorption isotherm was recorded at 77 K, where a Langmuir/BET surface area of activated MOF-650 was estimated to be 3230/2630 $m^2\ g^{-1}$ (Fig. 4a). The pore volume of MOF-650 is 1.18 $cm^3\ g^{-1}$, measured from the $N_2$ uptake at $P/P_0 = 0.95$.

### 4.4 Low pressure $H_2$ adsorption measurements

Low pressure hydrogen isotherms were recorded for activated MOF-649 and -650 at 77 and 87 K (Fig. 4b). As expected, MOF-649 displayed a Type I isotherm without a hysteresis loop, and no saturation uptake was observed under these experimental conditions. The $H_2$ uptake in MOF-649 was 7.0 mg $g^{-1}$ at 1 bar and 77 K (Fig. 4b). The $H_2$ uptake in MOF-650 outperforms MOF-649; MOF-650 demonstrated a $H_2$ uptake of 14.8 mg $g^{-1}$ at 77 K and 1 bar (Fig. 4b). From the fit of $H_2$ isotherms at 77 and 87 K, the coverage dependencies of the isosteric heats of adsorption ($Q_{st}$) for MOF-649 and MOF-650 were estimated. The initial $Q_{st}$ values of MOF-649 and MOF-650 were 5.3 kJ $mol^{-1}$ and 6.8 kJ $mol^{-1}$, respectively. The observed $Q_{st}$ of MOF-649 is in line with the value reported for isoreticular pillared MOFs suggesting a minor effect of azulene to improve the polarization potential required for the stabilization of $H_2$.[27] On the other hand, the initial $Q_{st}$ value for MOF-650 is superior when compared to the values obtained for representative MOF-5 (3.8–4.8 kJ $mol^{-1}$) and other MOFs having a pcu topology and $Zn_4O(CO_2)_6$ SBUs.[28–30]

### 4.5 Calculation of site-specific hydrogen adsorption energies in MOF-650 and IRMOF-8

For a better understanding of the adsorption properties and to investigate the reason for the observed higher $Q_{st}$ of MOF-650, we performed DFT-based calculations to model the $H_2$

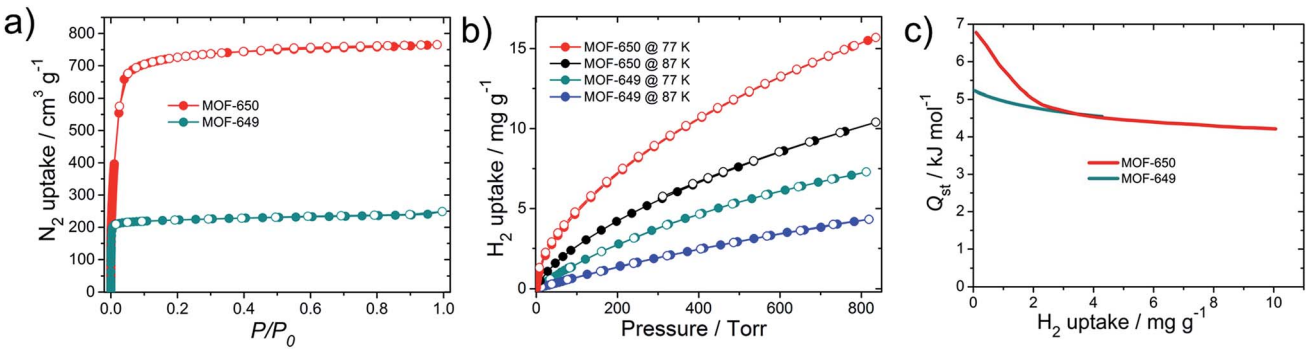


Fig. 4 $N_2$ (a) and $H_2$ (b) isotherms of the activated MOFs. Filled and open circles represent adsorption and desorption branches, respectively. Connecting traces are provided for better visualization of the sorption processes. (c) The coverage dependencies of adsorption enthalpies of $H_2$ in activated MOFs.

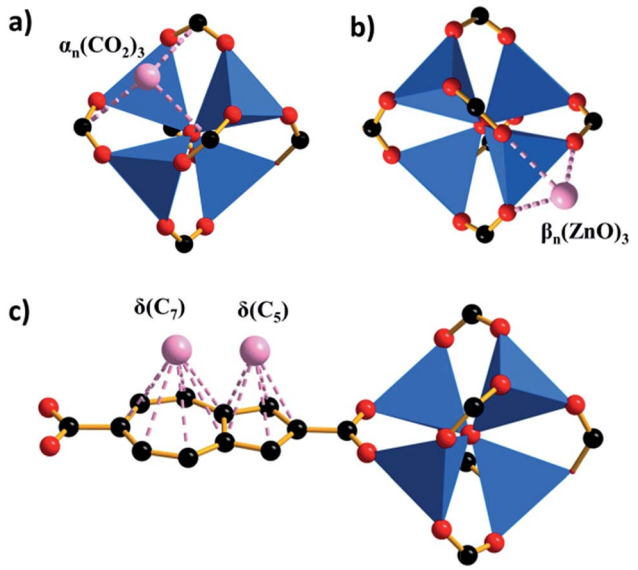


Fig. 5 Schematic representation of the investigated adsorption sites (visualized with light-pink spheres) in MOF-650 in $Pa\bar{3}$ or $F\bar{4}3m$. In panel (a), $\alpha_n$ (where $n = 1$–4) depicts one of the four α sites around the $Zn_4O(CO_2)_6$ unit and $n$ is distinct depending upon the number of 5- or 7-membered ring sides of azulene attached to the edge (see Section 4.2). In panel (b), $\beta_n$ (where $n = 1$–4) shows one of the four β sites around the $Zn_4O(CO_2)_6$ unit and again $n$ is distinct depending upon the number of 5- or 7-membered ring sides of azulene attached to the edge (see Section 4.2). (c) The view of the two different adsorption sites $\delta(C_7)$ and $\delta(C_5)$ located on the 7- and 5-membered rings of the azulene, respectively. Atom colors: Zn, blue polyhedra; O, red; C, black. H atoms are omitted for clarity.

adsorption. In particular, we considered the geometry and the energetics of the $H_2$ molecule when adsorbed at different primary binding sites within the framework of MOF-650 and IRMOF-8. These adsorption sites (Fig. 5) were selected on the basis of previous studies performed for related systems, which demonstrate preferred $H_2$ adsorption in the vicinity of the $(CO_2)_3$ structural unit and sites above the $(ZnO)_3$ face of a $ZnO_4$ tetrahedron.[11,12,31] Specifically, we selected four different sites in MOF-650 that were close to the $(CO_2)_3$ unit, *i.e.* $\alpha_1$–$\alpha_4$ and $(ZnO)_3$ units, *i.e.* $\beta_1$–$\beta_4$ (see Section 4.2, Fig. 2, and ESI for details†). In IRMOF-8 all α and β sites are respectively equivalent. In order to also take into account the adsorption at the linker itself, *i.e.* the δ site, we investigated two additional sites. The site closest to the 7-membered rings of azulene is labelled $\delta(C_7)$ and the one closest to the 5-member ring is labelled $\delta(C_5)$ (Fig. 5). In IRMOF-8, these sites are again equivalent, *i.e.* $\delta(C_6)$.[30]

Table 2 summarizes all the calculated adsorption energies for $H_2$ at the different sites for MOF-650 and IRMOF-8. At each site two conformations were considered for $H_2$: "parallel" (*i.e.* side-on interaction of $H_2$ with the plane of the adsorption site) and "perpendicular" (*i.e.* end-on interaction of $H_2$ with the plane of the adsorption site). The data clearly reveal that the most favourable adsorption occurs at the α sites followed by the β sites of MOF-650. The adsorption energies on the azulene linker (δ sites) are roughly 8 kJ $mol^{-1}$ and 1–2 kJ $mol^{-1}$ weaker in comparison to those at the α and β sites, respectively. The 5-membered ring, *i.e.* the $\delta(C_5)$ site, of MOF-650 binds $H_2$ more strongly than the 7-membered ring, *i.e.* the $\delta(C_7)$ site. This is in line with previously reported calculations conducted on unsubstituted azulene.[8] Notably, the adsorption energies in the vicinity of the $(CO_2)_3$ unit in MOF-650 are larger in comparison with those of IRMOF-8. This is especially true when considering the adsorption of the $H_2$ molecule in parallel configuration, in which the energies are demonstrated as superior – irrespective of the orientation of the adjacent azulene linkers. For the site $\delta(C_5)$ of MOF-650 the adsorption energy is slightly larger than at the delta (δ) site of IRMOF-8 when considering a perpendicular configuration of the adsorbed $H_2$ molecule. On the other hand, the calculated values for the β sites of MOF-650 are found to be a little lower than for IRMOF-8, in particular when the hydrogen molecule is adsorbed in parallel orientation (except at site $\beta_3$). $H_2$ mostly prefers a parallel orientation at α sites, and a perpendicular orientation at β sites, in both MOF-650 and IRMOF-8. Indeed, the calculated energy data clearly

Table 2 Binding energy of a single $H_2$ molecule when adsorbed at various sites in MOF-650 and IRMOF-8 either in perpendicular or in parallel orientation. Energies are given in kJ $mol^{-1}$

| Site | MOF-650 (perpendicular) | MOF-650 (parallel) | IRMOF-8 (perpendicular/parallel) |
|---|---|---|---|
| α | — | — | —[a]/−12.14 |
| $\alpha_1$ | −10.46 | −13.44 | —/— |
| $\alpha_2$ | −9.89 | −12.72 | —/— |
| $\alpha_3$ | —[a] | −13.71 | —/— |
| $\alpha_4$ | —[a] | −13.76 | —/— |
| β | — | — | −7.88/−7.34 |
| $\beta_1$ | −7.22 | −5.89 | —/— |
| $\beta_2$ | −7.27 | −6.76 | —/— |
| $\beta_3$ | —[a] | −7.95 | —/— |
| $\beta_4$ | −7.27 | −7.06 | —/— |
| $\delta(C_7)$ | −5.20 | −4.61 | —/— |
| $\delta(C_5)$ | −6.01 | −5.29 | —/— |
| $\delta(C_6)$ | —/— | —/— | −4.75/−4.81 |

[a] In these cases only the "parallel" configuration of $H_2$ was found to be stable after the structure was relaxed.

 

demonstrate that the incorporation of the azulene linker and its polarity influence the adsorption energies in a positive manner with the exception of some of the β sites. Thus, it is likely that the observed high $Q_{st}$ at zero coverage can be attributed to the $H_2$ adsorption at the α sites preferentially with a side-on (parallel) orientation.

## 5. Conclusions

A strategy has been pursued to improve the binding energy of hydrogen in metal–organic frameworks (MOFs) by incorporation of the internally polarized azulene system in comparison with the isomeric naphthalene system, thus creating polar pore walls. Two novel MOFs composed of internally polarized 2,6-azulenedicarboxylate (2,6-azd), termed MOF-649 [$Zn_2$(2,6-azd)$_2$(dabco), where dabco = 1,4-diazabicyclo[2.2.2]octane] and MOF-650 [$Zn_4O$(2,6-azd)$_3$], could be prepared. Both materials displayed permanent microporosity (Brunauer–Emmett–Teller surface areas of MOF-649 and MOF-650 were estimated to be 910 and 2630 $m^2\ g^{-1}$, respectively). The $H_2$ adsorption measurements revealed that MOF-650 adsorbs 14.8 mg $g^{-1}$ of hydrogen at 77 K and 1 bar. The polarization effect of the azulene unit in the framework is supported for MOF-650 by a high initial isosteric heat of adsorption of 6.8 kJ $mol^{-1}$. A detailed DFT analysis on MOF-650 helped to understand the site-specific interactions with hydrogen occurring preferably in sites around the $Zn_4O(CO_2)_6$ units in the energy range of 13 to 14 kJ $mol^{-1}$.

## Acknowledgements

Funding from the Swiss National Science Foundation (SNSF), University of Zurich and U.S. Department of Energy, BASF SE (Ludwigshafen, Germany) as well as generous computing resources from the University of Zurich are gratefully acknowledged. We thank Kyle Cordova (UC Berkeley) for his valuable comments.

## Notes and references

1 (*a*) M. Eddaoudi, D. B. Moler, H. Li, B. Chen, T. M. Reineke, M. O'Keeffe and O. M. Yaghi, *Acc. Chem. Res.*, 2001, **34**, 319; (*b*) O. M. Yaghi, M. O'Keeffe, N. W. Ockwig, H. K. Chae, M. Eddaoudi and J. Kim, *Nature*, 2003, **423**, 705; (*c*) S. Kitagawa, R. Kitaura and S.-I. Noro, *Angew. Chem., Int. Ed.*, 2004, **43**, 2334; (*d*) G. Feréy, *Chem. Soc. Rev.*, 2008, **37**, 191; (*e*) S. Ma, D. Sun, J. M. Simmons, C. D. Collier, D. Yuan and H.-C. Zhou, *J. Am. Chem. Soc.*, 2008, **130**, 1012; (*f*) J. Lee, O. K. Farha, J. Roberts, K. A. Scheidt, S. T. Nguyen and J. T. Hupp, *Chem. Soc. Rev.*, 2009, **38**, 1450; (*g*) C. Janiak and J. K. Vieth, *New J. Chem.*, 2010, **34**, 2366; (*h*) S. Ma and H.-C. Zhou, *Chem. Commun.*, 2010, **46**, 44; (*i*) J.-R. Li, R. J. Kuppler and H.-C. Zhou, *Chem. Soc. Rev.*, 2009, **38**, 1477; (*j*) H.-C. Zhou, J. R. Long and O. M. Yaghi, *Chem. Rev.*, 2012, **112**, 673; (*k*) H. Furukawa, K. E. Cordova, M. O'Keeffe and O. M. Yaghi, *Science*, 2013, **341**, 1230444.

2 (*a*) S. S. Kaye, A. Dailly, O. M. Yaghi and J. R. Long, *J. Am. Chem. Soc.*, 2007, **129**, 14176; (*b*) H. J. Park and M. P. Suh, *Chem.–Eur. J.*, 2008, **14**, 8812; (*c*) H. Furukawa, N. Ko, Y. B. Go, N. Aratani, S. B. Choi, E. Choi, A. Ö. Yazaydin, R. Q. Snurr, M. O'Keeffe, J. Kim and O. M. Yaghi, *Science*, 2010, **329**, 424; (*d*) O. K. Farha, O. Yazaydın, I. Eryazici, C. Malliakas, B. Hauser, M. G. Kanatzidis, S. T. Nguyen, R. Q. Snurr and J. T. Hupp, *Nat. Chem.*, 2010, **2**, 944; (*e*) H. J. Park, D.-W. Lim, W. S. Yang, T.-R. Oh and M. P. Suh, *Chem.–Eur. J.*, 2011, **17**, 7251.

3 (*a*) L. J. Murray, M. Dincă and J. R. Long, *Chem. Soc. Rev.*, 2009, **38**, 1294; (*b*) M. P. Suh, H. J. Park, T. K. Prasad and D.-W. Lim, *Chem. Rev.*, 2012, **112**, 782.

4 (*a*) M. Dincă and J. R. Long, *J. Am. Chem. Soc.*, 2005, **127**, 9376; (*b*) B. Chen, N. W. Ockwig, A. R. Millward, D. S. Contreras and O. M. Yaghi, *Angew. Chem., Int. Ed.*, 2005, **44**, 4745; (*c*) M. Dincă, A. Dailly, Y. Liu, C. M. Brown, D. A. Neumann and J. R. Long, *J. Am. Chem. Soc.*, 2006, **128**, 16876; (*d*) M. Latroche, S. Surblé, C. Serre, C. Mellot-Draznieks, P. L. Llewellyn, J.-H. Lee, J.-S. Chang, S. H. Jhung and G. Férey, *Angew. Chem., Int. Ed.*, 2006, **45**, 8227; (*e*) M. Dincă, W. S. Han, Y. Liu, A. Dailly, C. M. Brown and J. R. Long, *Angew. Chem., Int. Ed.*, 2007, **46**, 1419; (*f*) X.-S. Wang, S. Ma, P. M. Forster, D. Yuan, J. Eckert, J. J. López, B. J. Murphy, J. B. Parise and H.-C. Zhou, *Angew. Chem., Int. Ed.*, 2008, **47**, 7263; (*g*) Y.-G. Lee, H. R. Moon and P. Suh, *Angew. Chem., Int. Ed.*, 2008, **47**, 7741; (*h*) W. Zhou, H. Wu and T. Yildirim, *J. Am. Chem. Soc.*, 2008, **130**, 15268.

5 (*a*) S. S. Han and W. A. Goddard, *J. Am. Chem. Soc.*, 2007, **129**, 8422; (*b*) K. L. Mulfort and J. T. Hupp, *J. Am. Chem. Soc.*, 2007, **129**, 9604; (*c*) D. Himsl, D. Wallacher and M. Hartmann, *Angew. Chem., Int. Ed.*, 2009, **48**, 4639; (*d*) S. Yang, X. Lin, A. J. Blake, K. M. Thomas, P. Hubberstey, N. R. Champness and M. Schröder, *Chem. Commun.*, 2008, 6108.

6 (*a*) Y. Liu, J. F. Eubank, A. J. Cairns, J. Eckert, V. C. Kravtsov, R. Luebke and M. Eddaoudi, *Angew. Chem., Int. Ed.*, 2007, **46**, 3278; (*b*) D. F. Sava, V. C. Kravtsov, F. Nouar, L. Wojtas, J. F. Eubank and M. Eddaoudi, *J. Am. Chem. Soc.*, 2008, **130**, 3768.

7 S. Barman, H. Furukawa, O. Blacque, K. Venkatesan, O. M. Yaghi and H. Berke, *Chem. Commun.*, 2010, **46**, 7981.

8 (*a*) O. Hübner, A. Glöss, M. Fichtner and W. Klopper, *J. Phys. Chem. A*, 2004, **108**, 3019; (*b*) M. Wong, B. E. V. Kuiken, C. Buda and B. D. Dunietz, *J. Phys. Chem. C*, 2009, **113**, 12571.

9 M. Eddaoudi, J. Kim, N. Rosi, D. Vodak, J. Wachter, M. O'Keeffe and O. M. Yaghi, *Science*, 2002, **295**, 469.

10 (*a*) K. Seki and W. Mori, *J. Phys. Chem. B*, 2002, **106**, 1380; (*b*) K. Seki, S. Takamizawa and W. Mori, *Chem. Lett.*, 2001, **30**, 332; (*c*) K. Seki, *Chem. Commun.*, 2001, 1496; (*d*) D. N. Dybtsev, H. Chun and K. Kim, *Angew. Chem., Int. Ed.*, 2004, **43**, 5033; (*e*) H. Chun, D. N. Dybtsev, H. Kim and K. Kim, *Chem.–Eur. J.*, 2005, **11**, 3521; (*f*) H. C. Hoffmann, B. Assfour, F. Epperlein, N. Klein, S. Paasch, I. Senkovska, S. Kaskel, G. Seifert and E. Brunner, *J. Am. Chem. Soc.*, 2011, **133**, 8681; (*g*) N. Klein, H. C. Hoffmann, A. Cadiau, J. Getzschmann, M. R. Lohe, S. Paasch, T. Heydenreich,

K. Adil, I. Senkovska, E. Brunner and S. Kaskel, *J. Mater. Chem.*, 2012, **22**, 10303.
11 J. L. C. Rowsell, E. C. Spencer, J. Eckert, J. A. K. Howard and O. M. Yaghi, *Science*, 2005, **309**, 1350.
12 J. L. C. Rowsell, J. Eckert and O. M. Yaghi, *J. Am. Chem. Soc.*, 2005, **127**, 14904.
13 G. L. B. Carlson, F. H. Quina, B. M. Zarnegar and D. G. Whitten, *J. Am. Chem. Soc.*, 1975, **97**, 347.
14 M. V. Barybin, M. H. Chisholm, N. S. Dalal, T. H. Holovics, N. J. Patmore, R. E. Robinson and D. J. Zipse, *J. Am. Chem. Soc.*, 2005, **127**, 15182.
15 Agilent Technologies (formerly Oxford Diffraction), Yarnton, England, 2011.
16 H. Furukawa, M. A. Miller and O. M. Yaghi, *J. Mater. Chem.*, 2007, **17**, 3197.
17 A. L. Spek, *PLATON99 A Multipurpose Crystallographic Tool*, Utrecht University, Utrecht, 1999.
18 J. VandeVondele, M. Krack, F. Mohamed, M. Parrinello, T. Chassaing and J. Hutter, *Comput. Phys. Commun.*, 2005, **167**, 103.
19 *CP2K version 2.3 (Development Version)*, CP2K developers group, 2012, http://www.cp2k.org/.
20 Y. Zhang and W. Yang, *Phys. Rev. Lett.*, 1998, **80**, 890.
21 S. Grimme, J. Antony, S. Ehrlich and H. Krieg, *J. Chem. Phys.*, 2010, **132**, 154104.
22 J. VandeVondele and J. Hutter, *J. Chem. Phys.*, 2007, **127**, 114105.
23 S. Goedecker, M. Teter and J. Hutter, *Phys. Rev. B: Condens. Matter Mater. Phys.*, 1996, **54**, 1703.
24 K. Sillar, A. Hofmann and J. Sauer, *J. Am. Chem. Soc.*, 2009, **131**, 4143.
25 H. Li, M. Eddaoudi, M. O'Keeffe and O. M. Yaghi, *Nature*, 1999, **402**, 276.
26 K. Li, D. H. Olson, J. Y. Lee, W. Bi, K. Wu, T. Yuen, Q. Xu and J. Li, *Adv. Funct. Mater.*, 2008, **18**, 2205.
27 (*a*) J. Y. Lee, D. H. Olson, L. Pan, T. J. Emge and J. Li, *Adv. Funct. Mater.*, 2007, **17**, 1255; (*b*) Z. Wang, K. K. Tanabe and S. M. Cohen, *Chem.–Eur. J.*, 2010, **16**, 212.
28 (*a*) J. L. C. Rowsell and O. M. Yaghi, *J. Am. Chem. Soc.*, 2006, **128**, 1304; (*b*) B. Panella, M. Hirscher, H. Pütter and U. Müller, *Adv. Funct. Mater.*, 2006, **16**, 520.
29 A. Dailly, J. J. Vajo and C. C. Ahn, *J. Phys. Chem. B*, 2006, **110**, 1099.
30 J. I. Feldblyum, A. G. Wong-Foy and A. J. Matzger, *Chem. Commun.*, 2012, **48**, 9828.
31 E. C. Spencer, J. A. K. Howard, G. J. McIntyre, J. L. C. Rowsell and O. M. Yaghi, *Chem. Commun.*, 2006, 278.